

# Polarization-Dependent Study on Propagating Surface Plasmons in Silver Nanowires Launched by a Near-Field Scanning Optical Fiber Tip

Ning Liu, Zhipeng Li, and Hongxing Xu\*

Surface plasmons (SPs) have attracted great attention in recent years due to their potential applications in various fields of science and technology.<sup>[1]</sup> The possibility to confine light into subwavelength spatial dimensions through plasmonic structures allows integration of optical components beyond the limitation imposed by the diffraction of light. As one of the most important topics in integrated plasmonics, the propagation of surface plasmons has been investigated intensively, aiming to understand and harness the signal flow between different components within the plasmonic devices.

Due to their single-crystal structure, smooth surface, and well-defined geometry, chemically synthesized Ag nanowires (NWs) have been utilized as carriers for propagating surface plasmons in various applications, including single-photon detection,<sup>[2]</sup> remote excitation of fluorescence and surface enhanced Raman spectroscopy,<sup>[3]</sup> and signal routing in Ag NW branches.<sup>[4]</sup> A comprehensive understanding of the excitation of SP modes in cylindrical NWs is of pivotal importance to these applications. Recently, our group demonstrated that by changing the polarization of the incident light in the wire-end-launched configuration, different combinations of surface plasmon modes could be excited. Application of this technique in realizing various logical functions in Ag NW networks has been illustrated.<sup>[5]</sup> However, in some cases the light couples into propagating SP modes from the middle of the NW.<sup>[2,6]</sup> As the conservation of momentum prevents Gaussian-shaped light beams from coupling directly into the SP modes from the middle of the NW, SP propagation excited

this way usually involves near-field interaction or dipole active fluorescence coupling. Since the position of the coupling junctions or dipole emitters is usually fixed with respect to the nanowire, a systematic study on the influence of emitter location to the excitation of SP modes has not been reported with nanometer spatial precision. In this paper, we report a polarization-dependent study on SP modes excited through a near-field scanning optical fiber tip. The input light radiates out of the end of the fiber tip. Using a near-field raster scanning technique, the location of the emitter can be fully controlled and varied with nanometer accuracy. Our study shows that multiple SP modes in Ag NWs can be triggered through polarization-selective near-field interaction. The input coupling efficiency is modulated by Fabry-Perot interferences and the polarization plane of the resultant SP modes rotates around the central axis of the NW as the tip moves across the NW, leading to changes in the polarization of emission light at wire end.

The experiments were carried out with a commercial Nanonics Multiview 4000 system. This near-field scanning optical microscopy is based on a tapping-mode tuning fork atomic force microscopy (AFM) probe. The optical fiber tip, coated with thin films of Cr and Au and characterized by an exit aperture between 100 and 200 nm, is attached along the side of the tuning fork. The input laser light (CW 632.8 nm) is coupled into the optical fiber through an objective. The scanning stage is positioned underneath an upright Olympus optical microscope, equipped with a polarizer in the output light path and a DVC 710M CCD camera. Optical images are collected with a super-long working distance Nikon objective ( $\hat{1}100$ , NA = 0.7). A schematic of our experimental setup is shown in **Figure 1a**. Chemically synthesized Ag NWs were drop-cast on glass substrate from Ethanol solution. A 30 to 50 nm  $\text{Al}_2\text{O}_3$  film was deposited on the sample to protect it from oxidation.

Figure 1b shows a bright-field optical image of a silver NW with a diameter of 320 nm and a length of 17  $\mu\text{m}$ . The fiber tip at working distance (a few to tens of nanometers) from the sample surface and the input laser spot emerging from the end of tip are also visible. The corresponding dark-field image is given in Figure 1c and clearly reveals the emission of light from both ends of the Ag NW, generated by the propagating SP modes excited by the scanning tip. Instead of recording the emission of light with another optical fiber tip, the intensity of wire-end output is monitored with the CCD

Dr. N. Liu, Dr. Z. Li,<sup>[\*]</sup> Prof. H. Xu  
Nanoscale Physics and Devices Laboratory  
Beijing National Laboratory for  
Condensed Matter Physics  
and Institute of Physics  
Chinese Academy of Sciences  
PO Box 603-146, Beijing, 100190, PR China  
E-mail: hxxu@aphy.iphy.ac.cn

Prof. H. Xu  
Division of Solid State Physics/The Nanometer Consortium  
Lund University  
PO Box 118, Lund, S-221 00, Sweden  
[\*] Present address: Beijing Key Laboratory of Nano-Photonics  
and Nano-Structure (NPNS), Department of Physics, Capital Normal  
University, Beijing, PR China

DOI: 10.1002/sml.201101809



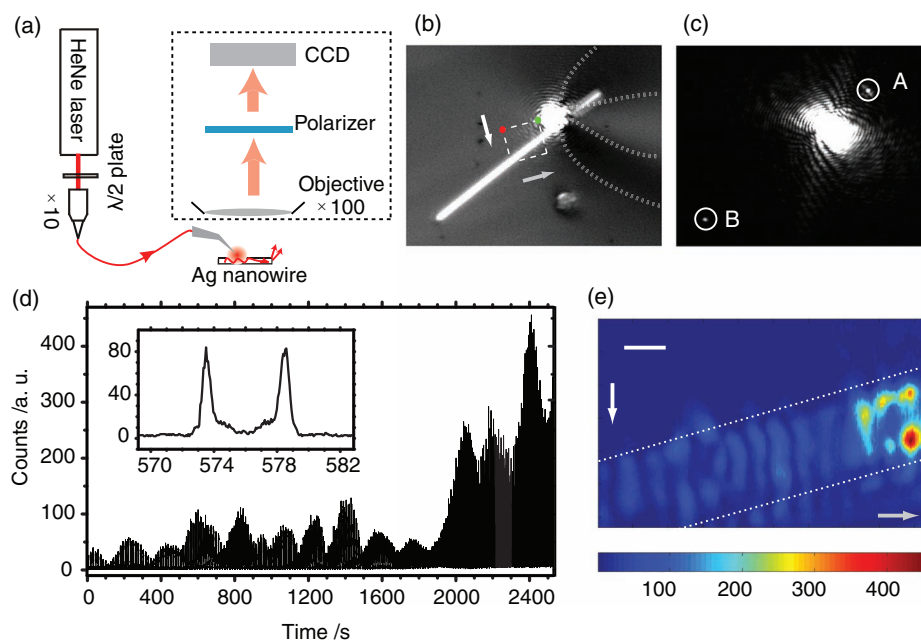


**Figure 1.** a) Schematic of the experimental setup. The microscope is indicated by a dashed rectangle. b) Bright-field optical image of an optical fiber tip with input radiation at working distance from a silver nanowire. The dotted curves outline the NSOM tip and its mirror image from the sample surface. The white dashed rectangle indicates the area that the tip scanned over to obtain (d), with the white arrow denoting the direction of each line scan (forward and backward), and the grey arrow indicating the second raster scanning direction. Red and green dots correspond to the starting ( $t = 0$  s) and ending positions ( $t \approx 2520$  s) of the tip for the entire scan. c) Corresponding dark-field image of (b), showing excited SPs scattering out as photons at the ends of wire. The emission spots are highlighted by white circles and indicated as A and B. d) Time trace of output intensity maximum in the area marked by A in panel (c), recorded by the CCD camera, as the tip scanned over the area indicated by the dashed white rectangle in panel (b). The inset shows part of the time trace, corresponding to the tip scanning across the NW and back to its starting position along the same scan line. e) The NSOM image converted from time trace (d). The scale bar in the image represents 500 nm. The white dashed lines outline the profile of the NW obtained by topographic imaging.

camera. An intensity–time trace obtained during raster scanning the tip over the portion of the NW marked by the dashed rectangle in Figure 1b is displayed in Figure 1d; the region from which the intensity is recorded is marked by a circle A in Figure 1c. The part of the time-trace corresponding to the tip moving forward and backward along a single line across the NW in the direction indicated by the white arrow in Figure 1b is shown in the inset of Figure 1d. The peaks in the curve are attributed to the excitation of SP propagation in the Ag NW, which is detected as photons scattered from the end of the wire. Since the tip position in the dashed rectangle is known at all time, the time-trace can be converted into a 2D false color image, as displayed in Figure 1e, where the lateral positions of the image represent the physical location of the tip. Contrary to standard near-field scanning optical microscopy (NSOM) images, which would show the spatial distribution of the electric field intensity along a NW at specific SP modes,<sup>[7]</sup> this image reveals the intensity change of the output light at wire-end as a function of tip position when it scans over part of the NW. With this method, the excitation of propagating SP and collection of output light are spatially separated and the polarization of emission light at wire-end can be interrogated with a conventional optical polarizer in the output light path. Both short- and long-period modulations are discerned in the image. These are attributed to Fabry-Perot interferences for

the short-range oscillation caused by the partial reflection of light at the wire end and the superposition of multiple SP modes for the beating of the long-range oscillation, respectively; the reasoning for this is detailed below.

The excitation mechanism of tip-induced SP propagation is quite different from the commonly used end-facet-launching scheme and is illustrated in **Figure 2**. Figure 2a describes the set of coordinates of NWs used in the following diagrams and simulations, with the center of the NW chosen as the origin. Similar to most near-field coupling cases, the input radiation is coupled into the propagating SP through optical mode overlap. When the tip is a few nanometers away from the NW, the electric field is maximized in the region of space between the fiber apex and the wire surface. Depending on the polarization of input radiation, the excited SP modes can be different. Both  $m = 0$  and  $m = 1$  SP modes are stimulated simultaneously for an electric field along the  $Z$ - and  $X$ -directions, as shown in Figure 2b. The percentage of each mode is determined by the best overlap of the mode profile of the superposition of the two modes with the input radiation. However, for electric field polarized along the  $Y$  direction, the  $m = -1$  mode is difficult to excite since the charge intensity maxima are off the symmetry axis defined by the tip and the center of the NW (Figure 2c), which leads to poor mode overlap.

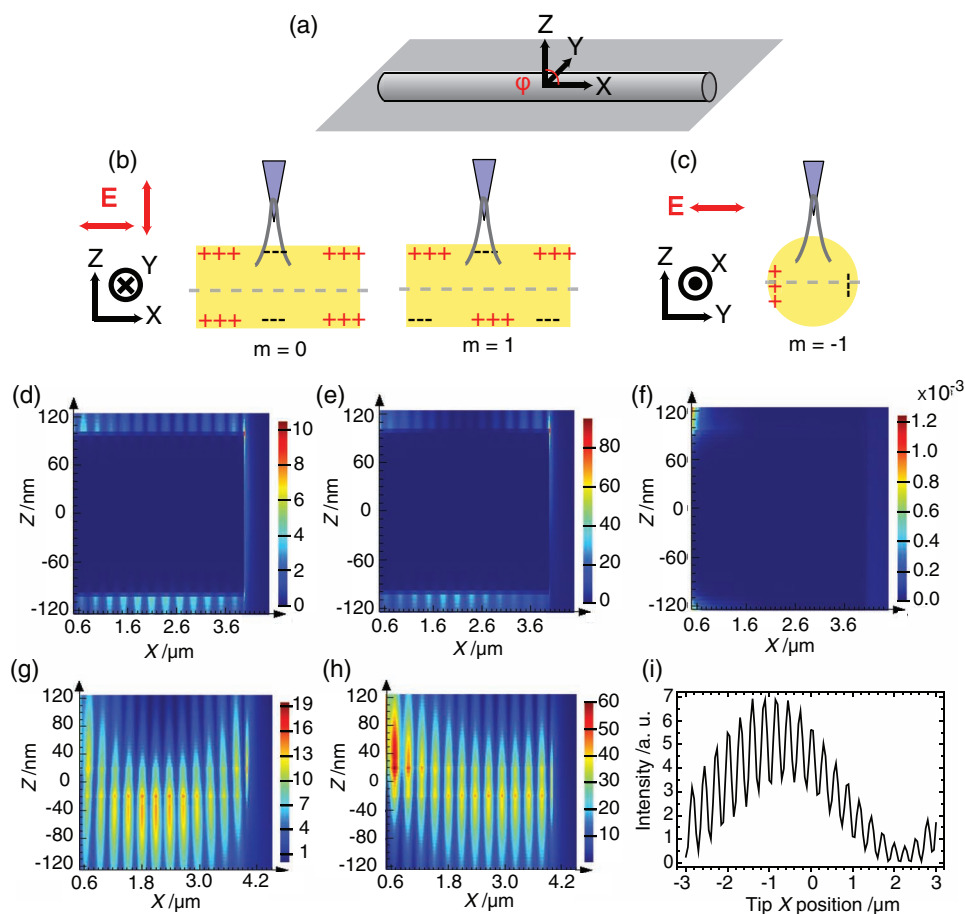


**Figure 2.** a) Coordinates of Ag NWs in simulation. The origin is located at the center of the NW and  $\varphi$  is the angle between the X- and Z-axes. b) Schematics of tip-induced SP modes in Ag NWs when the polarization of the input light is along the Z- and X-directions. ‘+’ and ‘-’ symbols denote the charge distribution within the wire. c)  $m = -1$  SP mode in Ag NW with Y input polarization. d–f) Electric field intensity plots of excited SP modes on the ZX plane passing the central axis of the NW when the dipole is placed at  $X = 0$ ,  $Y = 0$ ,  $Z = 110$  nm for polarization along X, Z, and Y directions, respectively. g–h) Intensity plots on the ZX plane at  $Y = -110$  nm for Z-polarized input radiation with dipole positioned at  $X = 0$  and  $X = 400$  nm, respectively. i) Output intensity maximum on XY plane at  $Z = 110$  nm, close to the wire end, as a function of input dipole position along the X-axis, at  $Y = 0$  and  $Z = 110$  nm.

To better estimate the input coupling efficiency at different input polarization direction, finite-difference time-domain simulations (Lumerical FDTD solutions) are used to evaluate the SP modes excited in each case. The tapered fiber tip is considered to be conical. Near-field simulation of the intensity of radiation scattered from the cone-end shows two peaks along the input polarization direction, suggesting a strong dipole component in the total electric field.<sup>[8]</sup> Also, both experimental and theoretical studies prove that the dipole term dominates in the far field regime.<sup>[9]</sup> Therefore, to simplify the input light profile and still include the essential physics, a point dipole was chosen here to model the input light source. In the simulation, the point dipole is positioned right above the middle of the NW and all three orthogonal polarization directions are considered. A wire of diameter 200 nm and length 8  $\mu\text{m}$  is used for the simulation to assure a reasonable calculation time. Figures 2d–f illustrate the intensity distribution of the electric field on the ZX plane, across the central axis of the NW, for the point dipole placed at  $X = 0$ ,  $Y = 0$ , and  $Z = 110$  nm and polarized along the X, Z, and Y directions, respectively. It is obvious from these plots that

the Z-polarized light can be most efficiently coupled into the propagating SP while almost no Y-polarized light couples into the SP modes. It is worth noting that our results qualitatively agree with the nanosphere-mediated near-field coupling case, which states that radially polarized input light could be coupled into the propagating SPs of Ag NWs most easily.<sup>[10]</sup> We also notice that instead of a chiral pattern,<sup>[11]</sup> the  $m = 0$  and  $m = 1$  modes excited by the X- or Z-polarized light form a beat pattern, as shown in Figure 2d and e, with the envelope maximum occurring alternately at the wire top and bottom. This is because the charge oscillation in  $m = 1$  mode is only along the Z-direction for both X- and Z-polarized input radiation. In addition, the relative phase between  $m = 0$  and  $m = 1$  modes is equal to zero at the point of excitation so that the envelope maximum of the beat always occurs at the tip location. As a result, when the dipole is displaced towards the end of the NW, the envelope maximum follows the position of the dipole and causes changes in output intensity at the wire-end, as shown in the simulations of Figure 2g and h, where the ZX-plane is chosen at  $Y = -110$  nm and the point dipoles are at  $X = 0$  and  $X = 400$  nm, respectively. Quite differently, the peak

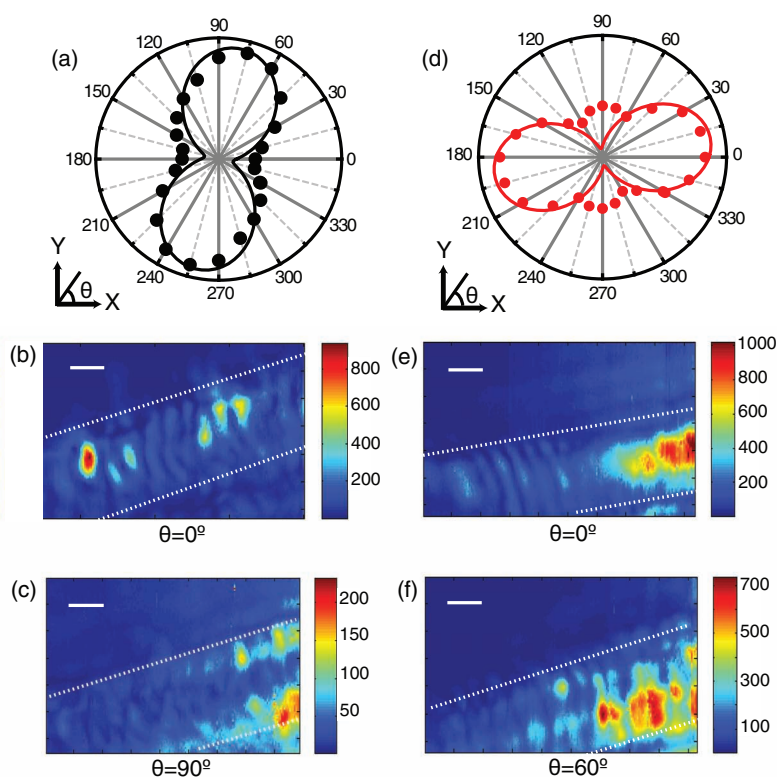


**Figure 3.** a,d) are the polarization measurements (solid circles) on two different input radiations. The solid curves are the fitted results to linear polarization. b,c) NSOM images for emission light polarized along  $0^\circ$  and  $90^\circ$ , respectively, with input polarization as shown in panel (a). e,f) NSOM images for emission components along  $0^\circ$  and  $60^\circ$ , respectively, with input polarization as shown in panel (d). White dotted lines outline the edges of the NW obtained from AFM topographic images. The scale bar is 500 nm.

and trough positions of the short-period oscillations, which are caused by the Fabry-Perot interference, are only determined by the geometry of the NW and do not change with the displacement of the tip along the  $X$ -direction (Figure 2g and h, and Figure S1 in the Supporting Information). The short-period intensity modulation seen at the output end is only related to the input coupling efficiency at the radiation gap. This can be understood as a result of constructive or destructive superposition of excited SPPs that are directly travelling to right (left) with the one first travelling to the left (right) and then being reflected back to the right (left) by the end facet of the NW. The phases between these two SPPs vary with the tip position, leading to enhancement or cancellation of the SPPs excited from the radiation gap, which gives rise to the short-range oscillations resolved in our experiment. Figure 2i shows the maximum intensity in the  $XY$ -plane, 10 nm above the NW and close to the end of wire, as a function of point dipole location along the  $X$ -direction. Both short- and long-range modulations are evident in this simulation, confirming the two main features observed in Figure 1e; however, the position of the actual envelope maximum cannot be correlated directly to the experimental data due to the difference in wire dimensions used in the simulation.

To gain a better understanding on how the tip-launched SP modes are affected by the tip apex position along the  $Y$ -direction, across the wire, incident and emission

polarization-dependent studies were carried out on the same NW, as shown in **Figure 3**. Figure 3a depicts the polarization of the scattered light from the end of tip, measured through the polarizer in the output light path. It is almost linearly polarized  $75^\circ$  off the long axis of the NW. The NSOM images in Figure 3b and c correspond to the emission light intensity polarized along the  $X$ - and  $Y$ -directions, respectively. It can be clearly seen that the intensity patterns change dramatically when different components of the output light are investigated. For the  $X$ -polarization, the signal is mostly concentrated in the upper middle part of the NW, while for the  $Y$ -polarization, the strongest intensity is found along the edges of the wire. When the input polarization is changed to that shown in Figure 3d, where a large portion of the input is polarized along the  $X$ -direction, two different output patterns are resolved, which are presented in Figure 3e and f, for output polarization along and at  $60^\circ$  off the  $X$ -axis, respectively. A spatial distribution symmetric along the long axis of the NW is obtained in the first case and the strongest signal is acquired with the tip positioned at the bottom half of the NW in the second case.

As already discussed in Figure 2, when the tip is positioned above the center of the NW ( $Y = 0$ ), only  $X$ - or  $Z$ -polarized light can be coupled efficiently into propagating SP modes. Based on the same principles, when the tip moves toward the edges of the NW, for polarization direction perpendicular to NW, the only component that can be coupled into SP modes is along the radial direction defined by the tip location, as denoted by the dashed grey line in **Figure 4a**. Consequently, the  $m = 1$  SP mode excited by the scanning tip rotates by the same amount around the central axis of the NW. Figure 4b and c show simulation results of the electric field intensity distribution in the  $XY$ -plane, 10 nm above the NW, and  $ZX$ -plane, 10 nm away from the end of NW, with the tip positioned at  $Y = 0$ ,  $Z = 110$  nm, and the input dipole polarized in the  $Z$ -direction. Figure 4d and e correspond to the simulations for a tip positioned at  $Y = 80$  nm and  $Z = 80$  nm with the same polarization. It can be clearly observed that the long-range modulation and emission pattern at the end of the wire both rotate around the  $X$ -axis. In addition, since we keep the same input polarization directions (along  $Z$ ), the input coupling efficiency decreases (as does the emission intensity at wire-end) when the tip moves to the edges of the NW, as demonstrated in Figure 4c and e. On the other hand, for an  $X$ -polarized input dipole, the long-range beat pattern rotates around the central axis, when the tip moves to the edges of the NW; however, the input coupling efficiency is unchanged and same amount of SP modes are excited in the NW (Figure S2 in the Supporting Information).

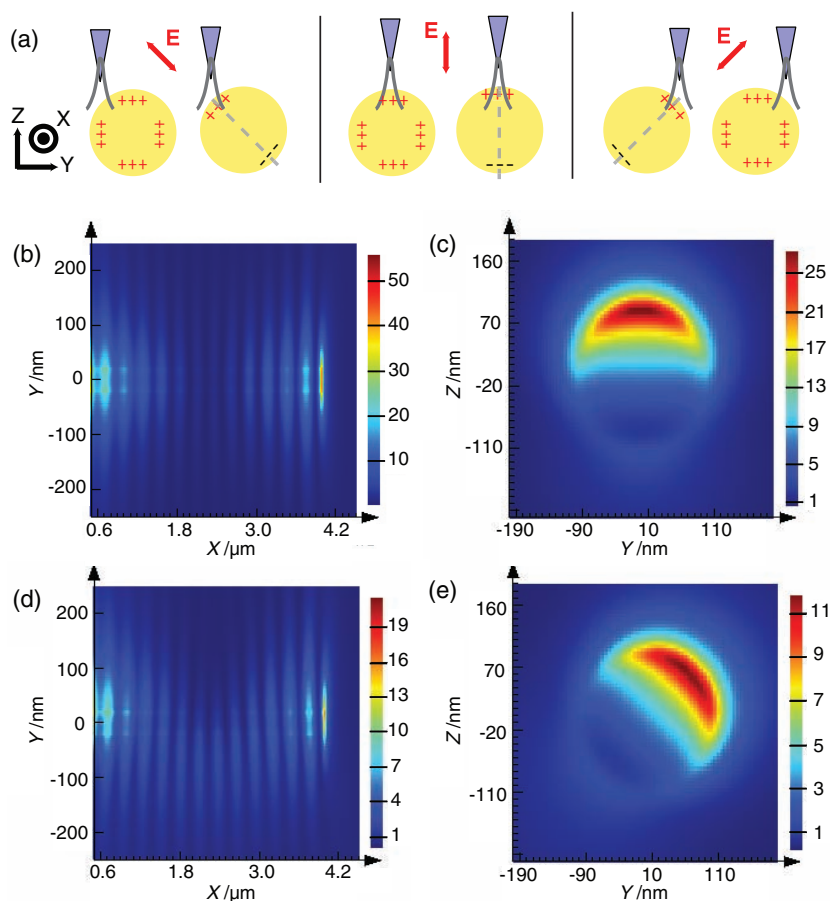


**Figure 4.** a) Schematics of the changes in tip-launched SP modes as the tip moves across the NW with input dipole polarized perpendicular to the central axis of the wire. The red arrows denote the radial polarization direction defined by the tip position. b,c) Intensity plots on the XY-plane at  $Z = 110$  nm and on the YZ-plane at  $X = 4.01$   $\mu\text{m}$ , respectively, with input dipole polarized along the Z-direction and positioned at  $Y = 0$ ,  $Z = 110$  nm. d,e) are the corresponding XY and YZ plots when the input dipole of the same polarization is positioned at  $Y = 80$  nm and  $Z = 80$  nm.

One thing worth noting is that using a polarizer after the objective to measure the polarization direction of light makes the Z-component in input radiation ‘invisible’. From the near-field simulation of the output radiation of light from a NSOM fiber tip,<sup>[8]</sup> we know that the Z-component of the electric field at the tip end is not null even with X- or Y-linearly polarized input light at the other end of the fiber. Furthermore, the scanning tip in our experiment is not mounted vertically to the sample plane (as shown in Figure 1b). As a result, there should be Z-component at the radiation gap for all incident polarizations.

With these considerations in mind, it is now easier to interpret the NSOM images presented in Figure 3. According to Li et al.,<sup>[12]</sup> for SPP oscillating along the Z-direction, the emitted light is polarized along the X-direction; for oscillation along the Y-direction, the emission light is polarized along the Y-direction. As already discussed earlier, for perpendicularly polarized (with respect to the NW) incident light, only a radial component defined by the tip location can be coupled into SP modes. Hence, it is easier to excite Y-polarized emission light when the tip is placed at the edges of the NW, as

confirmed by Figure 3c. On the contrary, to maximize the X-component in the emission light, the tip needs to be positioned close to  $Y = 0$ . The slight asymmetry in Figure 3b is explained by reasoning that the total input polarization includes both Y- and Z-components; therefore the preferred tip position to achieve the best coupling efficiency is off-centered.

For the X-polarized incident light, the coupling efficiency is the same for all tip locations, therefore the output intensity in a specific polarization direction is only determined by the rotation angle of the beat pattern around the central axis of the NW. The maximum output intensity along the X-direction is reached when the tip is at  $Y = 0$  and symmetrically decreases as the tip moves to the edges, as displayed in Figure 3e. For output polarization  $\theta = 60^\circ$ , the intensity is maximized when the preferred tip location is  $60^\circ$  from the Y-direction, corresponding to tip scanning over the lower part of the NW.

In summary, we have demonstrated that, for the near-field fiber tip launching method, multiple SP modes are excited simultaneously via mode overlap at the radiation gap. Our results show that Fabry-Perot interference can lead to significant changes in input coupling efficiency and the superposition of multiple SP modes gives rise to a beat-like modulation in the output intensity at the wire-end. Moreover, input coupling is highly polarization selective. For electric field perpendicular to the long axis of the NW, only radially polarized light can be effectively coupled

into the propagating SPs. This also means that the preferred input polarization direction is position sensitive. Consequently, the emission polarization depends on the location of input radiation. Our results provide valuable information on how different SP modes can be excited and transferred through near-field interconnection in plasmonic NWs and the aspects people need to pay attention to during the plasmonic or hybrid photonic-plasmonic circuit design. Subwavelength manipulation on the interconnect position can lead to great changes in the coupling efficiency, suggesting the possibility of building nanoscale optical circuits in the future. Furthermore, our study could also enrich the understanding on how the dipole active excitons can decay into various modes of propagating SPs, which is of great importance to fluorescence- and gain-related plasmonic devices.

## Experimental Section

NSOM multi-mode optical fiber tips (CFN-200 MV4000) were purchased from Nanonics. The emission light from wire-end was captured with a DVC 710M camera and processed using DVCView

software. The region of interest was selected by a circle and the time-trace of the maximum intensity within the area recorded by the software. The polarization of light radiated out of the end of the fiber tip was obtained by measuring the polarization of reflected input light from the glass slide through the polarizer in the output light path.

## Supporting Information

Supporting Information is available from the Wiley Online Library or from the author.

## Acknowledgements

This work was supported by a MOST Grant (2009CB930700), NSFC Grants (Nos.10625418, 10874233, 11004237, 11134013, and 10904171), the "Knowledge Innovation Project" (KJCX2-EW-W04) of CAS, and the Beijing Natural Science Foundation (Grant No. 1122012).

- [1] a) R. F. Oulton, V. J. Sorger, T. Zentgraf, R.-M. Ma, C. Gladden, L. Dai, G. Bartal, X. Zhang, *Nature* **2009**, *461*, 629; b) A. Hartschuh, E. J. Sanchez, X. S. Xie, L. Novotny, *Phys. Rev. Lett.* **2003**, *90*, 095503; c) J. Henzie, M. H. Lee, T. W. Odom, *Nat. Nanotechnol.* **2007**, *2*, 549; d) H. X. Xu, M. Käll, *Sens. Actuat. B-Chem.* **2002**, *87*, 244.

- [2] A. V. Akimov, A. Mukherjee, C. L. Yu, D. E. Chang, A. S. Zibrov, P. R. Hemmer, H. Park, M. D. Lukin, *Nature* **2007**, *450*, 402.
- [3] Y. Fang, H. Wei, F. Hao, P. Nordlander, H. X. Xu, *Nano Lett.* **2009**, *9*, 2049.
- [4] Y. R. Fang, Z. P. Li, Y. Z. Huang, S. P. Zhang, P. Nordlander, N. J. Halas, H. X. Xu, *Nano Lett.* **2010**, *10*, 1950.
- [5] a) H. Wei, Z. P. Li, X. Tian, Z. Wang, F. Cong, N. Liu, S. Zhang, P. Nordlander, N. J. Halas, H. X. Xu, *Nano Lett.* **2011**, *11*, 471; b) H. Wei, Z. X. Wang, X. R. Tian, M. Käll, H. X. Xu, *Nat. Commun.* **2011**, *2*, 387.
- [6] a) M. W. Knight, N. K. Grady, R. Bardhan, F. Hao, P. Nordlander, N. J. Halas, *Nano Lett.* **2007**, *7*, 2346; b) X. Guo, M. Qiu, J. Bao, B. J. Wiley, Q. Yang, X. Zhang, Y. Ma, H. Yu, L. Tong, *Nano Lett.* **2009**, *9*, 4515; c) Y. Ma, X. Li, H. Yu, L. Tong, Y. Gu, Q. Gong, *Opt. Lett.* **2010**, *35*, 1160–1162.
- [7] H. Ditzbacher, A. Hohenau, D. Wagner, U. Kreibitz, M. Rogers, F. Hofer, F. R. Aussenegg, J. R. Krenn, *Phys. Rev. Lett.* **2005**, *95*, 257403.
- [8] A. Drezet, M. J. Nasse, S. Huant, J. C. Woehl, *Europhys. Lett.* **2004**, *66*, 41.
- [9] a) C. Obermuller, K. Karrai, *Appl. Phys. Lett.* **1995**, *67*, 3408; b) J. Meixner, W. Andrewjeski, *Ann. Phys.* **1950**, *7*, 157.
- [10] F. Hao, P. Nordlander, *Appl. Phys. Lett.* **2006**, *89*, 103101.
- [11] S. P. Zhang, H. Wei, K. Bao, U. Håkanson, N. J. Halas, P. Nordlander, H. X. Xu, *Phys. Rev. Lett.* **2011**, *107*, 096801.
- [12] Z. P. Li, Y. R. Fang, Y. Z. Huang, P. Nordlander, H. X. Xu, *Nano Lett.* **2010**, *10*, 1831.

Received: September 2, 2011  
Revised: February 13, 2012  
Published online: June 25, 2012